

SCIENTIFIC REPORTS



OPEN

Synthesis and characterization of vertically standing MoS₂ nanosheets

Han Li¹, Huaqiang Wu^{1,2}, Shuoguo Yuan³ & He Qian^{1,2}

Received: 01 December 2015

Accepted: 18 January 2016

Published: 18 February 2016

Molybdenum disulfide (MoS₂) has been attracting much attentions due to its excellent electrical and optical properties. We report here the synthesis of large-scale and uniform MoS₂ nanosheets with vertically standing morphology using chemical vapor deposition method. TEM observations clearly reveal the growth mechanism of these vertical structures. It is suggested that the vertical structures are caused by the compression and extrusion between MoS₂ islands. More importantly, the vertical morphology of two dimensional (2D) materials hold many promising potential applications. We demonstrate here the as-synthesized vertically standing MoS₂ nanosheets could be used for hydrogen evolution reaction, where the exchange current density is about 70 times of bulk MoS₂. The field emission performance of vertically standing MoS₂ were also improved due to the abundantly exposed edges.

Graphene has attracted extensive interests in various research fields since it was obtained through mechanical exfoliation by Novoselov *et al.* in 2004¹. Due to the distinctive physical properties of one-layer thin 2D materials compared with their bulk counterparts^{2,3}, layered materials have attracted much attentions, such as transition metal dichalcogenides (TMDCs)⁴, transition metal oxides⁵, boron nitride (BN)⁶, *etc.* Lots of efforts have been made by using 2D materials in the fields of microelectronics^{7,8}, optoelectronics⁹, sensors¹⁰ and energy storage^{11,12}. However, these works have been devoted to utilize 2D materials lying flat on the substrates. Less of attention has been paid on their alternative configuration^{13–15}. Amongst these nanometric architectures, vertically standing 2D materials hold great potential in many applications due to their high aspect ratio and extensively exposed edges¹⁶.

For example, the minimized dimension and vertically aligned morphology of 2D materials consequently enable the fabrication of mini-sized energy storage devices with high capacity and high packing density, such as hydrogen storage devices, batteries and supercapacitors. The exposed edges with dangling bonds are chemical active and may play an important role in many catalytic reactions, such as hydrodesulfurization, hydrogen evolution reaction (HER) *etc.*^{17–20}. J. Shi *et al.*²⁰ demonstrate that the HER activity relates closely to the edge sites of MoS₂ flakes and the basal surfaces are catalytically inert, revealing the importance of exposed edges in catalytic reactions²¹. Furthermore, It has been demonstrated that vertically growth 1D nanotubes/nanowires and 2D nanosheets with atomically thin edges can significantly improve the field emission properties^{22,23}, making vertically standing 2D materials promising candidates in field emission applications^{24–26}.

There have already been lots of works based on the one dimensional (1D) nanowires and nanotubes. And the growth mechanism for vertical 1D nanowires and nanotubes are widely discussed. Normally, nanowires and nanotubes are assumed to be grown at the interface between catalytic and nanowires (nanotubes) via vapor-liquid-solid (VLS) or vapor-solid-solid (VSS) process in 1D growth^{27,28}. In contrast, the growth mechanisms for vertically standing 2D materials are still vague. L. Jiang *et al.*²⁴ demonstrated that a transition from 2D complete films to 3D clusters beyond a critical layer thickness may be caused by the sufficient accumulation of strain energy and the defects of the as-deposited film during vertical graphene growth process. J. Zhao *et al.*²⁹ demonstrated that vertically standing graphene could be nucleated from the buffer layer or from the surface of carbon onions. However, there are no clear evidences demonstrating that how these transitions from 2D films to 3D clusters happened. We believe that a clear understanding of the growth mechanism would facilitate the

¹Institute of Microelectronics, Tsinghua University, Beijing, China. ²Tsinghua National Laboratory for Information Science and Technology (TNList), Beijing, China. ³Department of Applied Physics, The Hong Kong Polytechnic University, Hong Kong, China. Correspondence and requests for materials should be addressed to H.W. (email: wuhq@tsinghua.edu.cn)

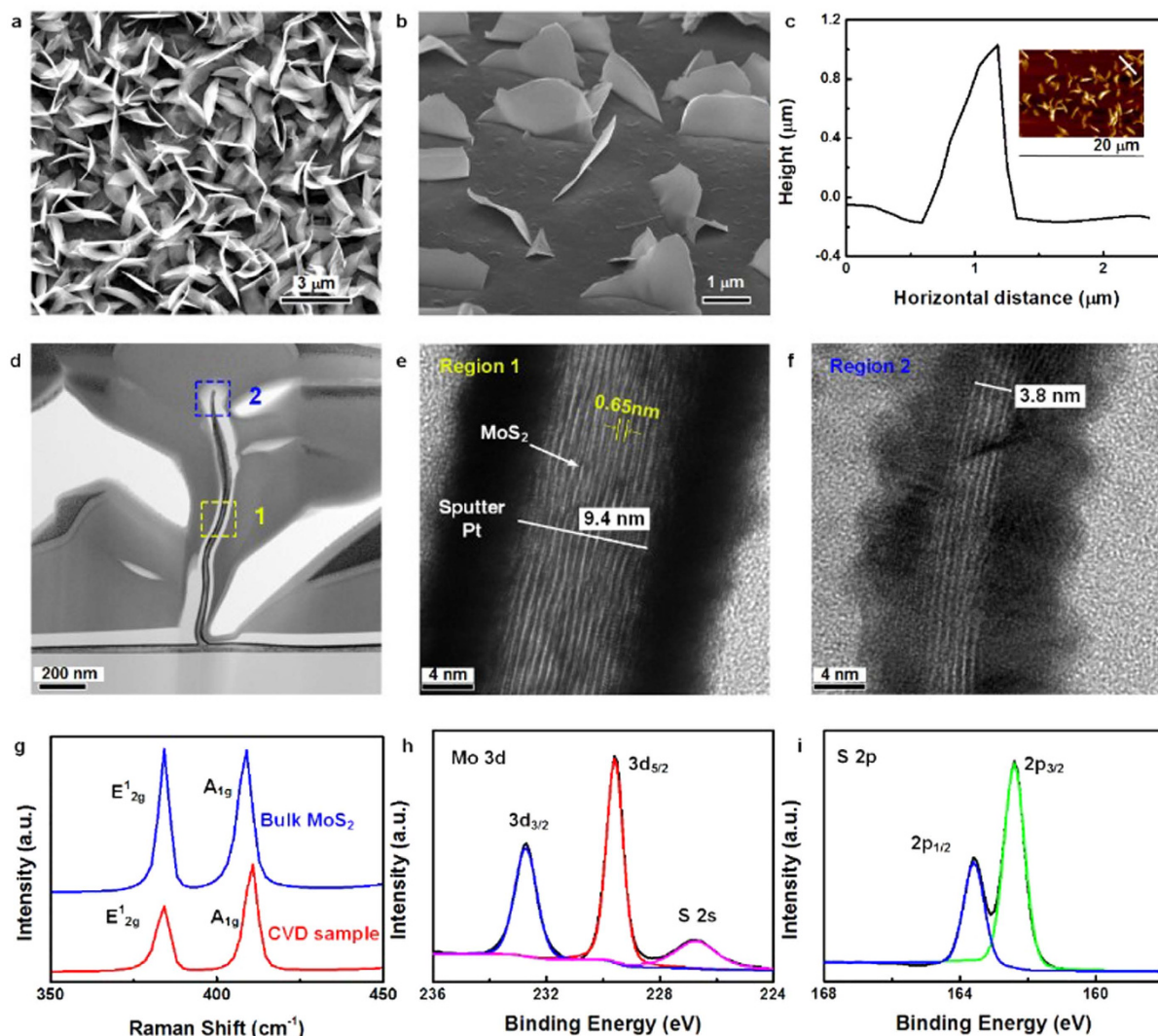


Figure 1. Characterization of as-synthesized MoS₂ nanosheets. (a) Top view FE-SEM image of vertically standing MoS₂ nanosheets. (b) 52.5° tilt view of MoS₂ nanosheets which clearly show the vertically standing feature. (c) AFM height profile of MoS₂ nanosheets, the insert shows the corresponding AFM image. (d) Cross-sectional TEM image of vertically standing MoS₂ grown on SiO₂/Si substrate. (e) Region1 (yellow block in d): High-magnification cross-sectional TEM image of MoS₂ layers, clearly shows the layered structure of MoS₂ nanosheets. (f) Region2 (blue block in d): High-magnification cross-sectional TEM images on the top of vertically standing MoS₂ nanosheets, and nanometric edge with size of several nanometers could be observed. (g) Raman spectrum of our sample and single-crystal bulk MoS₂ obtained by mechanical exfoliation. (h) XPS spectra of Mo 3d and S 2s peaks. (i) XPS spectra of S 2p peak.

development of vertically standing materials based applications. In addition, the growth mechanism could also promote the process in designing more complex nanometric structures.

In this work, we propose a method to synthesize vertically standing MoS₂ nanosheets using a conventional chemical vapor deposition (CVD) method. Various characterizations techniques were used to give a deep analysis of those vertically standing MoS₂ nanosheets. In addition, a possible mechanism is proposed based on the experimental results. Furthermore, the field emission properties and the HER performance of vertically standing MoS₂ nanosheets were reported.

Results

Synthesis and characterization of vertically standing MoS₂. A typical SEM image of the vertically standing MoS₂ nanosheets grown on SiO₂/Si substrate is shown in Fig. 1a. It clearly shows that MoS₂ nanosheets were uniformly grown on the substrate. The 52.5° tilt SEM image (Fig. 1b) demonstrates that the as-grown MoS₂ nanosheets are nearly perpendicular to the substrate. AFM height profile is shown in Fig. 1c, where the corresponding AFM image is shown in the inset. The nanometric edges of different MoS₂ layers could be clearly observed in the high magnification SEM image (see Supplementary Fig. S1 online). It is believed that these

nanometric protrusions and edges are catalytically active sites which could significantly enhance the catalytic and field emission properties.

To further explore the microstructure and quality of the as-grown MoS₂ nanosheets, cross-section TEM analysis were carried out. TEM samples were prepared using Focused Ion Beam (FIB) process. The cross-section TEM image (Fig. 1d) shows the general morphologies of a vertically free standing MoS₂ nanosheets grown on SiO₂/Si substrate. The synthesized MoS₂ nanosheet stands nearly perpendicularly upon the substrate, and the height of this MoS₂ sheet is about 1.1 μm. High resolution TEM images are shown in Fig. 1e,f, corresponding to the region 1 and 2 marked in Fig. 1d respectively, where layered structure of MoS₂ could be clearly observed. The distance between two MoS₂ layers was measured to be about 0.65 nm (Fig. 1e), which is consistent with previous reports^{7,30}. The thickness of MoS₂ tip was measured to be 3.8 nm, corresponding to 5 layers of MoS₂. It's worth to note that the thickness of MoS₂ nanosheet is non-uniform. The thickness of MoS₂ increased from 3.8 nm to be 9.4 nm in the middle region of the sheet (Fig. 1e,f), revealing a tapered morphology of MoS₂ nanosheets. More morphology TEM images could be found in the Supplementary Fig. S2. The same morphology observation was reported in the free-standing vertical graphene by Zhao *et al.*²⁹ It's believed that these pyramid-like shape was caused by the terraces and steps formed during the growth, which also maintain the stability of the vertical structure.

MoS₂ nanosheets were also characterized using Raman spectroscopy. A typical Raman spectrum of our CVD grown MoS₂ sample is displayed in Fig. 1g. Two Raman characteristic bands at 410 and 384 cm⁻¹ with the full-width-half-maximum (FWHM) values of 5.8 and 5.9 cm⁻¹ could be found, corresponding to the out-of-plane A_{1g} and in-plane E_{2g}¹ vibration of MoS₂ respectively^{30–32}. Figure 1g also presents the Raman spectrum of a single-crystal bulk MoS₂ obtained by mechanical exfoliation as a reference. The similar value of FWHM between CVD samples and pristine MoS₂ reveals the high quality of CVD grown MoS₂. Note that the Raman peak corresponding to the out-of-plane mode (A_{1g}) is determined by sulfur atoms vibrating along c axis while the in-plane E_{2g}¹ mode are seen to involve motions of molybdenum and sulfur atoms in the basal plane³³. Thus it can be inferred that there are more exposed edges in the MoS₂ films grown by CVD than those obtained by mechanical exfoliation. Figure 1h,i display detailed XPS spectrum of Mo and S binding energies. The survey scan is provided in Supplementary Fig. S3. None oxidized Mo or S is found after the examination of Mo and S peaks.

Growth mechanism for vertically standing MoS₂ nanosheets. To elucidate the growth mechanism of these vertically standing MoS₂ nanosheets, different samples with varied growth time were prepared and examined. After 2 minutes growth in 750 °C, many speck-like features could be observed (Fig. 2a), and it is believed that those spots are the nucleation sites for horizontal growth of monolayer MoS₂ films. With growth time continued, most seeds grew into larger domain sizes and some seeds merged into one uniform film, and some triangular MoS₂ islands were formed on top of MoS₂ films at the same time (Fig. 2b). More triangle-shaped MoS₂ islands were formed above MoS₂ films after 5 minutes growth (Fig. 2c), after that, a transformation from 2D growth to 3D growth started (Fig. 2d). Raman spectroscopy analysis have been applied on those samples with different growth time. As shown in Supplementary Fig. S4, the intensity ratios between A_{1g} and E_{2g}¹ modes of CVD grown MoS₂ nanosheets samples are higher than that of bulk MoS₂ samples, revealing a higher density of exposed edges in those CVD grown MoS₂ nanosheets samples. With growth time increased from 5 minutes to 10 minutes, the ratio between A_{1g} and E_{2g}¹ mode intensity was also increased, suggesting a transformation from 2D to 3D growth.

More SEM observations were performed on the intermediate state of MoS₂ nanosheets to find out how these vertical MoS₂ nanosheets are formed. It could be observed in Fig. 2e,f that MoS₂ seedlings are originated from the aggregation zone of different MoS₂ islands. Thus, it can be inferred from the SEM observations that the formation of vertical structures were caused by the interaction between different MoS₂ islands. Cross-section TEM of a vertical MoS₂ nanosheet (Fig. 2g) exhibits this nanosheets originates from a thick MoS₂ film at the bottom. High resolution TEM image (Fig. 2h) shows the thick MoS₂ film has clear layered structure. From the TEM observations, it could be observed that the vertical MoS₂ nanosheet are originated from the MoS₂ island layers. Based on above results, it could be inferred that vertical standing MoS₂ seedlings may originate due to the curling force introduced by the increasing defects and strain energy³⁴. Figure 2i display the nanobeam electron diffraction (NBD) pattern from Fig. 2h (selected area marked by the circle), which shows only regularly arranged diffraction spots, corresponding to the hexagonal crystal structure of MoS₂.

TEM analyses were performed on the collision or distortion area where the vertically standing MoS₂ nanosheets nucleated from. Basically, two kinds of vertical morphology and their corresponding base structure were observed (Fig. 3). It can be clearly observed in the TEM images that the vertical MoS₂ nanosheets were grown from the buffer layer underneath on both cases. The first kind of vertical morphology is shown in Fig. 3a,b. The MoS₂ nanosheets are originated from the buffer layers and formed by the extension and the curl of the plane MoS₂ buffer layers. Alternatively, the vertical structure could be originated from the merge of two separated MoS₂ films (Fig. 3e,f). The formation of vertical morphology may be caused by the collision between two MoS₂ islands. The same triangular structure could be clearly observed at the intermediate state as shown in Supplementary Fig. S5. In addition, the stable triangle could be observed on the bottom structure on other TEM observations. Energy-dispersive X-ray spectroscopy (EDX) (see Supplementary Fig. S6 online) certify that nearly no chemical elements are existed in the triangle area, suggesting that the empty triangle was formed due to the curl of MoS₂ films instead of other chemical reaction. We believe that the self-formative triangular area could enhance the stability of the whole vertical structure.

Based on the above observations, a vertical growth mechanism is proposed to explain the formation of vertically standing MoS₂ nanosheets. It is believed that the intensive compression between different MoS₂ islands cause the collision and slide of MoS₂ plates, which induce the vertical structure growth. As shown in Fig. 3c,d, when a high barrier of MoS₂ islands or plates block the extension of MoS₂ islands, the MoS₂ islands may slip and change to vertical growth. Alternatively, when two MoS₂ island push and collide against each other, the compression force may produce obvious distortion that an arch structure could be formed to release the pressure (Fig. 3g,h), which

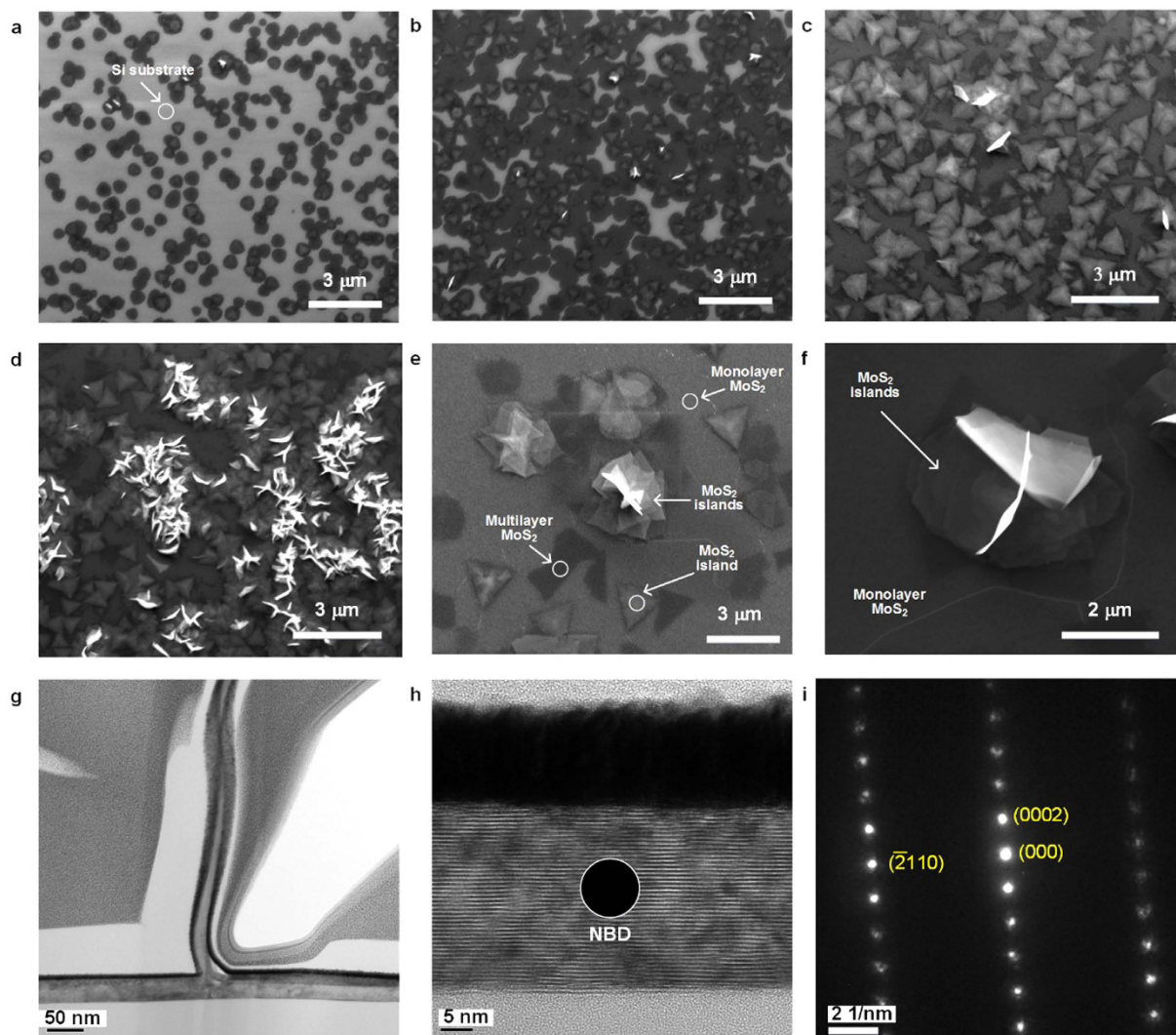


Figure 2. SEM and TEM observation on the formation of vertically standing MoS₂ nanosheets.

(a–d) SEM images of the MoS₂ films grown at the same condition but with different growth time: (a) 2 minutes, (b) 3 minutes, (c) 5 minutes and (d) 7 minutes. (e–f) SEM observations on the initial stage of the vertical MoS₂ formation. (g) Cross-sectional TEM image of vertically standing MoS₂. (h) HR-TEM image of plane MoS₂ nanosheets. (i) NBD pattern from h (selected area marked by the circle).

would subsequently act as the growth template for the vertical growth of MoS₂ nanosheets. Because vertical MoS₂ are associated with MoS₂ islands, it could be inferred that the alignment of vertically standing MoS₂ nanosheets would be improved by synthesizing unanimous MoS₂ islands with constant growth direction. MoS₂ growth orientation has been reported to be facet-dependent³⁵. Thus, the alignment might be improved by choosing a specific substrate.

To better understand the growth model, schematic graphs are shown in Fig. 4a–e. During the growth period, firstly, MoO₃ powder was partially reduced by sulfur vapor to form volatile MoO_{3-x} or gaseous MoS₂ and these sub-oxide compounds or gaseous MoS₂ were adsorbed and diffused to the substrate, and subsequently formed nucleation sites of MoS₂ films (Fig. 4a)³⁶. With growth time increased, separated 2D MoS₂ films were generally formed due to the growth and merging of the seeds as illustrated in Fig. 4b. It has been shown that the concentration of the gaseous MoS₂ or sub-oxide compounds is an important thermodynamics and kinetics factor for the MoS₂ growth³⁷. Due to the high concentration of the reactants introduced by the fast evaporation of sulfur powder in our experiment (see Methods), the growth of MoS₂ films would be facilitated by the supersaturated MoS₂ vapor and sub-oxide compounds vapor. And multi-layer MoS₂ films were consequently formed with increasing growth time. After that, MoS₂ films are grown in a layer-by-layer fashion until a certain critical thickness (Fig. 4c). And then MoS₂ islands were formed (Fig. 4d) to get an energetic favorable morphology according to the Stranski-Krastanov (SK) growth model^{38,39}. With growth continued, MoS₂ islands quickly extended and merged. A high strain energy would be introduced due to the fast chemical reaction. Thus, MoS₂ seedlings could originate from the collision or distortion area of different MoS₂ islands as shown in Fig. 4e. It is worth to note that though vertically standing MoS₂ could originate from different based structures, the growth direction and the dominated surface facets remain the same: with ±(002) planes defining the two dominant surfaces (see Fig. 4f). The observed

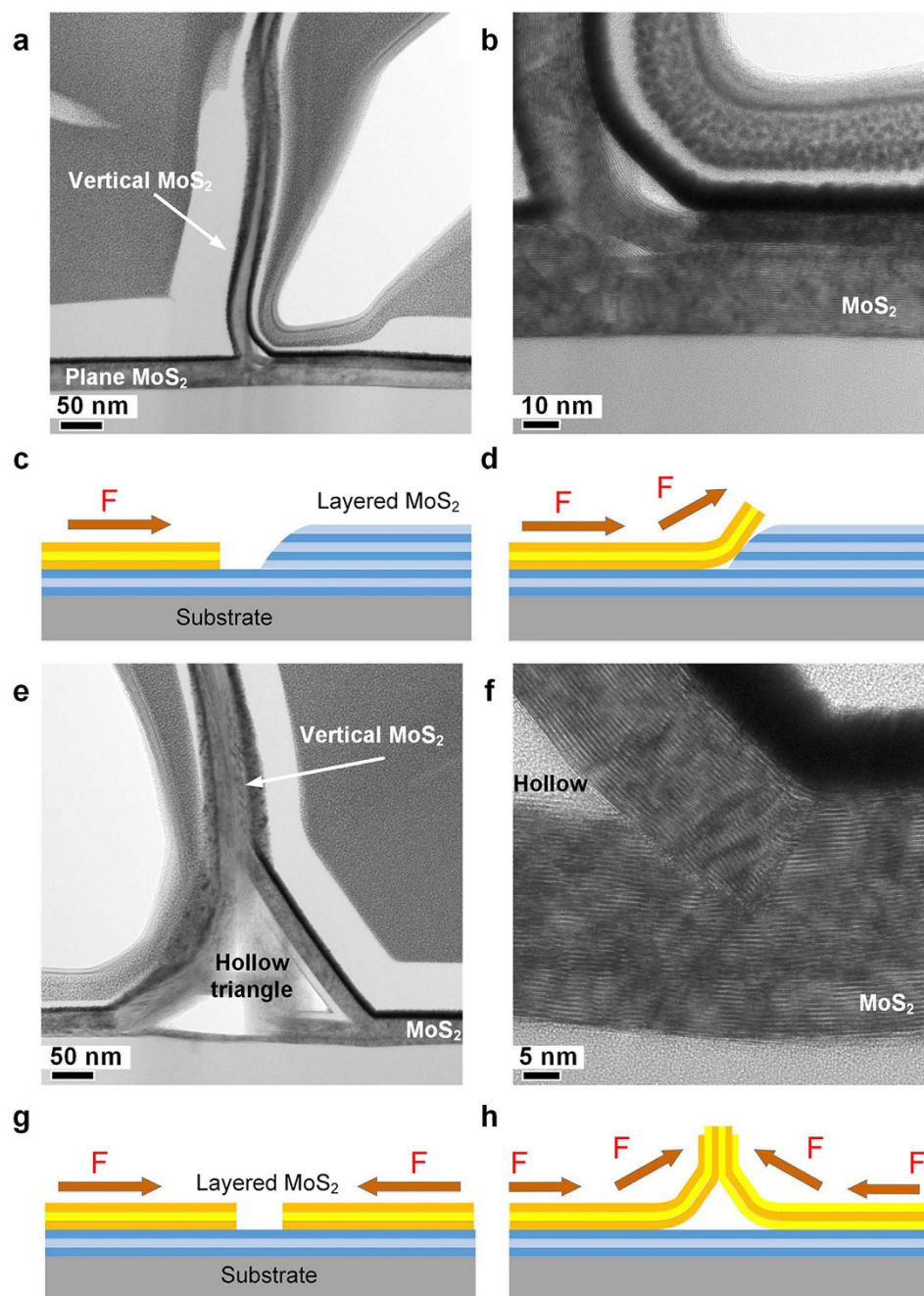


Figure 3. Two types of vertical morphologies and their corresponding structure models. (a–d) Type I and their corresponding models. (e–h) Type II and their corresponding models.

morphologies of the MoS₂ are driven by the requirement for reducing surface energy. Such a {002}-dominant surface structure is caused by the lowest surface-energy of (002) surface, which is consistent with previous report⁴⁰.

HER and field emission performance. To evaluate the catalytic activity of vertically standing MoS₂ nanosheets, a typical three-electrode setup was used for HER test. Vertically standing MoS₂ nanosheets were deposited on gold films using the same CVD method as described previously (see Supplementary Fig. S7 online). Typical cathodic polarization curves and corresponding Tafel plots are shown in Fig. 5a,b. The polarization curve of bare gold electrodes is also given in Fig. 5a. As it is known, Tafel slope is determined by the rate-limiting step of HER⁴¹. The Tafel slope in our sample was measured to be about 92 mV/decade (Fig. 5b). Previous studies have shown a large range of Tafel slope from 40 mV to 140 mV/dec and the reaction mechanism on MoS₂ still remains inconclusive^{18–21,42,43}.

The charge-transfer resistance could be estimated by using electrochemical impedance spectroscopy (EIS) method, revealing a lower charge-transfer resistance than gold films (see Supplementary Fig. S8 online). The

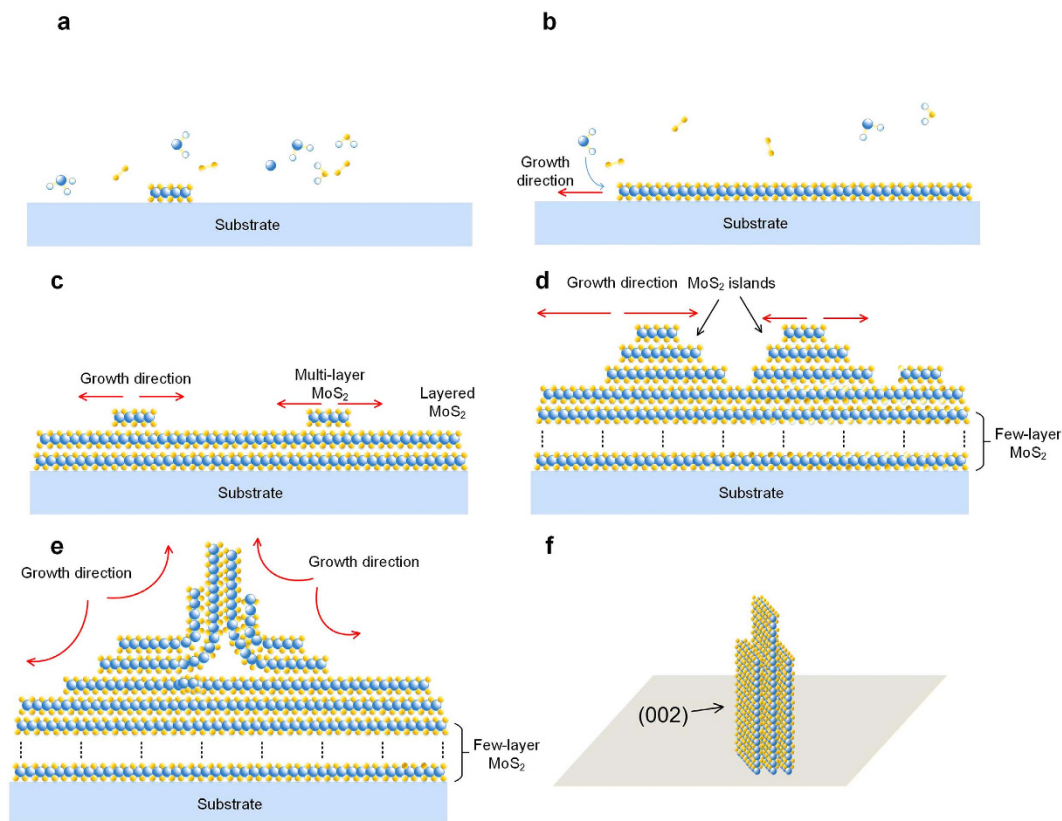


Figure 4. Growth model of vertically standing MoS₂ nanosheets. (a) “Nucleation stage”: nucleation sites were formed due to the reaction of MoO_{3-x} and S. (b) Two-dimensional MoS₂ film was generally formed due to the growth and merge of seeds and bilayer MoS₂ sheets were formed due to the continuous supply of reactant. (c) Multi-layer MoS₂ films were generally formed. (d) MoS₂ islands were formed beyond a certain critical MoS₂ layers and their interaction may cause the accumulation of deformation energy. (e) The vertically standing MoS₂ nanosheets may formed due to the horizontal and vertical compression and dilatation caused by the regional compression. (f) The simplified model for “vertical MoS₂ nanobelts”.

exchange current density, j_0 , is determined by fitting the linear portion of Tafel plot at low cathodic current to the Tafel equation (see Supplementary Fig. S9 online). Based on the results, it is found the exchange current density j_0 is about 22.3 $\mu\text{A}/\text{cm}^2$, which is 70 times of bulk MoS₂⁴⁴. The large value of j_0 is due to the high density of exposed edges^{20,21}. However, the interlayer hopping of electrons between different MoS₂ layers may limit the HER performance of vertically aligned MoS₂ nanosheets^{42,45}. Thus we believe the overall performance of our samples could be further improved by introducing doping during CVD process, which will be explored in the future. Another important criterion for a good electrocatalyst is its high durability. To evaluate this, continuous cyclic voltammograms were performed. The polarization curves before and after 1000 cycle are shown in Fig. 5c, where negligible loss of cathodic current could be observed.

In order to characterize the field-emission properties of vertically standing MoS₂ nanosheets, a series of field emission measurement experiments were performed (Fig. 6). The anode was an indium tin oxide (ITO)-coated glass, and the vertically standing MoS₂ nanosheets grown on SiO₂/Si substrate was used as the cathode. Figure 6a shows the field-emission current versus electric field of the as-prepared MoS₂ nanosheets. The turn-on electric field ($J = 10 \mu\text{A}/\text{cm}^2$) is around 2.46 V/ μm , which is smaller than previous reported MoS₂ nanosheets ($\sim 2.8\text{--}5.5 \text{ V}/\mu\text{m}$)^{25,46,47}. Fowler-Nordheim (FN) theory is the most commonly used model for understanding the electron-emission behaviour of various nanostructures. A modified F-N equation is used here to analyze the field emission property of MoS₂, which could be expressed as:

$$J = \lambda_M a \phi^{-1} E^2 \beta^2 \exp(-v_F b \phi^{-3/2} / \beta E) \quad (1)$$

Where $a = 1.54 \times 10^{-6} \text{ A eV V}^{-1}$ is a constant which depends on the surface structure and $b = 6.83 \times 10^7 \text{ V cm}^{-1} \text{ eV}^{-3/2}$, J is the emission current density, E is the applied average field, ϕ is the work function of emitter, λ_M is the macroscopic pre-exponential correction factor and v_F (correction factor) is a particular value of the principal Schottky-Nordheim barrier function v^48 . The ratio of the actual local electric field and the applied average electric field is known as the field enhancement factor β . Fig. 6b shows the $\ln(J/E^2)$ versus $1/E$ curve which has good agreement with the FN equation. The field-enhancement factor β of the vertical standing MoS₂ sheets was calculated to be 6240 by taking the work function ϕ of bulk MoS₂ to be 4.3 eV⁴⁹. The large enhancement factor is due to the nanometric protrusions and sharp edges as we observed in Fig. 1.

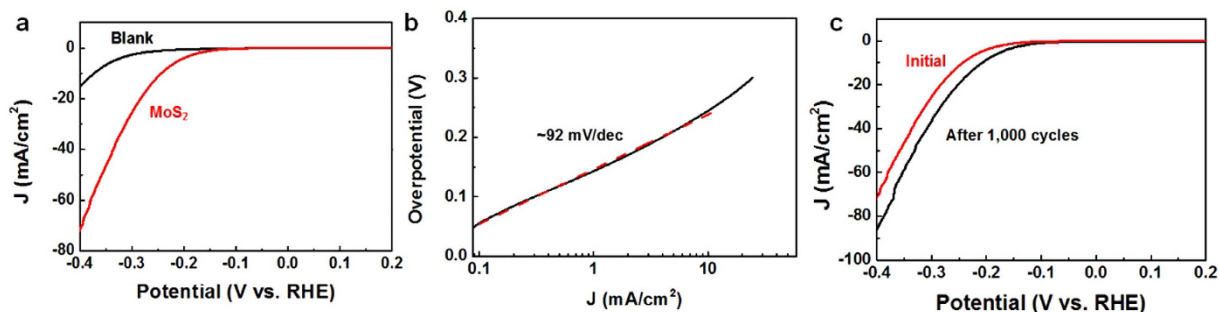


Figure 5. Electrochemical characterization of vertically standing MoS₂ nanosheets. (a,b) Polarization curves and corresponding Tafel plots of as-grown vertically standing MoS₂ films on Au foils. (c) Durability test for the as-grown sample.

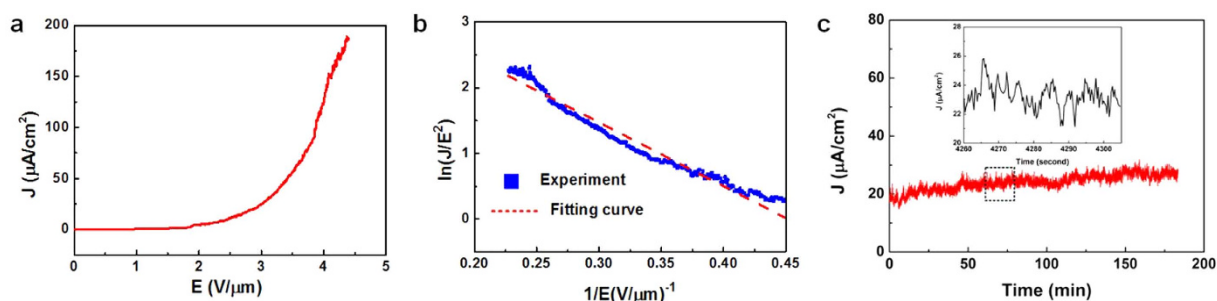


Figure 6. Field emission performance of vertically standing MoS₂ nanosheets. (a) Electron field emission current as a function of applied electric field. (b) The corresponding Fowler-Nordheim ($\ln(J/E^2)$ vs $1/E$) plot. (c) Field emission current stability curves of the MoS₂ nanosheets. The inset shows the change of current density in detail. The sampling interval is 200 ms in both picture.

The stability of emission current from the vertically standing MoS₂ nanosheets was also measured (Fig. 6c). A stable emission current density of about 22 $\mu\text{A}/\text{cm}^2$ over 170 min was recorded without any indication of degradation. Some spike like fluctuations were observed. The main reason of these fluctuations are believed to be caused by the adsorption/desorption and ion bombardment of residual molecules during the high field⁵⁰. This test shows fairly stable emission current from vertically standing MoS₂ nanosheets. The SEM observations on MoS₂ nanosheets after field emission were carried out and shown in Supplementary Fig. S10. No severe deterioration of emitter surface was observed, demonstrating the stability of MoS₂ nanosheets during field emission process.

Discussion

We have developed a CVD process for synthesizing vertically standing MoS₂ nanosheets. High density MoS₂ nanosheets with sharp edges could be synthesized. TEM observations on the nucleation sites reveal the growth mechanism for the based structure of vertically standing MoS₂. The based structures act as the growth templet and promote the subsequently vertical growth of MoS₂ nanosheets. It is suggested that the high strain energy caused by the compression between MoS₂ islands are the main reason for vertically standing MoS₂ nanosheets growth. These MoS₂ nanosheets exhibit enhanced field-emission properties with low turn-on electric field and good emission stability, suggesting promising in field emission based devices applications. In addition, we further confirmed the catalytic activity in HER. A high exchange current density of $\sim 28 \mu\text{A}/\text{cm}^2$ is achieved, which is caused by high density of the exposed edge sites. More generally, the ultrathin material, that is, the three-atoms-thick MoS₂, together with its vertical morphology, would hold great promising potential in catalytic, sensor, field emission applications.

Methods

Growth method. The MoS₂ growth was performed in a conventional quartz tube. Silicon substrates with 285 nm SiO₂ layer were cleaned in Piranha solution, followed by acetone, isopropanol and deionized bath for 5 minutes, and then finally dried using nitrogen gas. After that, samples were mounted on top of a quartz boat and faced down above high purity MoO₃ powder (14 mg, 99.998%, Alfa Aesar). Also, 120 mg sulfur powder (99.5%, Alfa Aesar) was placed in a separate quartz boat located in the upstream of the quartz tube. The distance between sulfur powder and MoO₃ powder was kept at 13 cm. After that, the tube was pumped down to base pressure ($< 0.1 \text{ Pa}$) and flushed with high purity nitrogen repeatedly. The tube was then filled with 1000 sccm nitrogen until one-atmosphere. During the synthesis process, the MoO₃ was heated up to 750 °C at a rate of 15 °C/min in an argon environment at atmospheric pressure for 10 min. 5 sccm N₂ was used as a carrying gas. Meanwhile, the sulfur was sublimated rapidly at approximately temperature of 700 °C. After growth procedure, the substrate was cooled down rapidly. Supplementary Fig. S11 shows the schematic diagram of the CVD equipment used in this study.

Characterization. The surface morphology which reveals the coverage and uniformity of the grown MoS₂ nanosheets was observed directly by SEM (Quanta FEG 450). Raman spectroscopy (Horiba, LabRAM HR-800), atomic force microscopy (AFM, Veeco Nanoscope IIIa) and transmission electron microscopy (TEM, FEI Tecnai G2 F20) were used to further characterize structure and quality of the as-grown MoS₂ nanosheets.

A diode setup in a vacuum chamber was adopted for field emission tests. The prepared samples were placed as the cathode and an indium tin oxide (ITO)-coated glass was used as the anode. Five 150- μm -thick and electrically insulating alumina films were used as spacers, making the distance between the cathode and anode at 250 μm (see Supplementary Fig. S12 online). The base pressure of the vacuum chamber was kept at 1×10^{-4} Pa. The emission current versus the applied voltage were characterized automatically by a Keithley 2410 sourcemeter and a high voltage DC power supply. The field emission current stability was investigated using a computer controlled data acquisition system.

In order to evaluate the catalytic effects of those vertically standing MoS₂ nanosheets, the HER tests were carried out. All of the electrochemical measurements were performed in 0.5 M H₂SO₄ solution using a three-electrode setup on an electrochemical workstation, with a saturated calomel electrode as the reference electrode (SCE), MoS₂ nanosheets grown on Au films the working electrode and a Pt foil the counter electrode. It was calibrated with respect to reversible hydrogen electrode (RHE). The calibration was performed in the high purity H₂ saturated electrolyte with two Pt foils as the working electrode and counter electrode. In 0.5 M H₂SO₄, $E(\text{RHE}) = E(\text{SCE}) + 0.252$ V. All the potentials reported in our manuscript are against RHE. Linear sweep voltammetry was conducted with a scan rate of 5 mV/s. And AC impedance measurement was carried out at an overpotential (η) of 0.12V with an AC voltage of 5 mV.

References

- Novoselov, K. S. *et al.* Electric field effect in atomically thin carbon films. *Science* **306**, 666–669 (2004).
- Kuc, A., Zibouche, N. & Heine, T. Influence of quantum confinement on the electronic structure of the transition metal sulfide TS₂. *Phys. Rev. B* **83** (2011).
- Mak, K. F., Lee, C., Hone, J., Shan, J. & Heinz, T. F. Atomically Thin MoS₂: A New Direct-Gap Semiconductor. *Phys. Rev. Lett.* **105** (2010).
- Ramakrishna Matte, H. S. S. *et al.* MoS₂ and WS₂ Analogues of Graphene. *Angew. Chem.* **122**, 4153–4156 (2010).
- Osada, M. & Sasaki, T. Two-dimensional dielectric nanosheets: novel nanoelectronics from nanocrystal building blocks. *Adv. Mater.* **24**, 210–228 (2012).
- Dean, C. R. *et al.* Boron nitride substrates for high-quality graphene electronics. *Nat. Nanotechnol.* **5**, 722–726 (2010).
- Radisavljevic, B., Radenovic, A., Brivio, J., Giacometti, V. & Kis, A. Single-layer MoS₂ transistors. *Nat. Nanotechnol.* **6**, 147–150 (2011).
- Cui, X. *et al.* Multi-terminal transport measurements of MoS₂ using a van der Waals heterostructure device platform. *Nat. Nanotechnol.* **10**, 534–540 (2015).
- Splendiani, A. *et al.* Emerging photoluminescence in monolayer MoS₂. *Nano Lett.* **10**, 1271–1275 (2010).
- Liu, B. *et al.* High-Performance Chemical Sensing Using Schottky-Contacted Chemical Vapor Deposition Grown Monolayer MoS₂ Transistors. *ACS nano* **8**, 5304–5314 (2014).
- Putungan, D. B., Lin, S. H., Wei, C. M. & Kuo, J. L. Li adsorption, hydrogen storage and dissociation using monolayer MoS₂: an ab initio random structure searching approach. *Phys. Chem. Chem. Phys.* **17**, 11367–11374 (2015).
- Acerce, M., Voiry, D. & Chhowalla, M. Metallic 1T phase MoS₂ nanosheets as supercapacitor electrode materials. *Nat. Nanotechnol.* **10**, 313–318 (2015).
- Romo-Herrera, J. M., Terrones, M., Terrones, H., Dag, S. & Meunier, V. Covalent 2D and 3D networks from 1D nanostructures: designing new materials. *Nano Lett.* **7**, 570–576 (2007).
- Wang, P. P., Sun, H., Ji, Y., Li, W. & Wang, X. Three-dimensional assembly of single-layered MoS₂. *Adv. Mater.* **26**, 964–969 (2014).
- Yu, J. H. *et al.* Vertical heterostructure of two-dimensional MoS(2) and WSe(2) with vertically aligned layers. *Nano Lett.* **15**, 1031–1035 (2015).
- Jiang, S. *et al.* Vertical ultrathin MoS₂ nanosheets on a flexible substrate as an efficient counter electrode for dye-sensitized solar cells. *Nanoscale* **7**, 10459–10464 (2015).
- Xu, X., Faglioni, F. & Goddard, W. A. Methane activation by transition-metal oxides, MO_x (M = Cr, Mo, W; x = 1, 2, 3). *J. Phys. Chem. A* **106**, 7171–7176 (2002).
- Jaramillo, T. F. *et al.* Identification of active edge sites for electrochemical H₂ evolution from MoS₂ nanocatalysts. *Science* **317**, 100–102 (2007).
- Li, Y. *et al.* MoS₂ nanoparticles grown on graphene: an advanced catalyst for the hydrogen evolution reaction. *J. Am. Chem. Soc.* **133**, 7296–7299 (2011).
- Shi, J. *et al.* Controllable growth and transfer of monolayer MoS₂ on Au foils and its potential application in hydrogen evolution reaction. *ACS Nano* **8**, 10196–10204 (2014).
- Kong, D. *et al.* Synthesis of MoS₂ and MoSe₂ films with vertically aligned layers. *Nano Lett.* **13**, 1341–1347 (2013).
- Huang, C. K., Ou, Y. X., Bie, Y. Q., Zhao, Q. & Yu, D. P. Well-aligned graphene arrays for field emission displays. *Appl. Phys. Lett.* **98** (2011).
- Huang, H. *et al.* Field electron emission of layered Bi₂Se₃ nanosheets with atom-thick sharp edges. *Nanoscale* **6**, 8306–8310 (2014).
- Jiang, L. *et al.* Controlled synthesis of large-scale, uniform, vertically standing graphene for high-performance field emitters. *Adv. Mater.* **25**, 250–255 (2013).
- Kashid, R. V. *et al.* Enhanced field-emission behavior of layered MoS₂ sheets. *Small* **9**, 2730–2734 (2013).
- Hallam, T., Cole, M. T., Milne, W. I. & Duesberg, G. S. Field emission characteristics of contact printed graphene fins. *Small* **10**, 95–99 (2014).
- Kodambaka, S., Tersoff, J., Reuter, M. C. & Ross, F. M. Germanium nanowire growth below the eutectic temperature. *Science* **316**, 729–732 (2007).
- Wang, N., Cai, Y. & Zhang, R. Q. Growth of nanowires materials Science and Engineering *R. Reports* **60**, 1–51 (2008).
- Zhao, J., Shaygan, M., Eckert, J., Meyyappan, M. & Rummeli, M. H. A growth mechanism for free-standing vertical graphene. *Nano Lett.* **14**, 3064–3071 (2014).
- Li, H. *et al.* From Bulk to Monolayer MoS₂: Evolution of Raman Scattering. *Adv. Funct. Mater.* **22**, 1385–1390 (2012).
- Late, D. J., Liu, B., Matte, H. S. S. R., Rao, C. N. R. & Dravid, V. P. Rapid Characterization of Ultrathin Layers of Chalcogenides on SiO₂/Si Substrates. *Adv. Funct. Mater.* **22**, 1894–1905 (2012).
- Thripuranthaka, M., Kashid, R. V., Sekhar Rout, C. & Late, D. J. Temperature dependent Raman spectroscopy of chemically derived few layer MoS₂ and WS₂ nanosheets. *Appl. Phys. Lett.* **104**, 081911 (2014).
- Verble, J. L. & Wieting, T. J. Lattice Mode Degeneracy in MoS₂ and Other Layer Compounds. *Phys. Rev. Lett.* **25**, 362–& (1970).

34. Zhu, M. Y. *et al.* A mechanism for carbon nanosheet formation. *Carbon* **45**, 2229–2234 (2007).
35. Shi, J. *et al.* Substrate Facet Effect on the Growth of Monolayer MoS₂ on Au Foils. *ACS nano* **9**, 4017–4025 (2015).
36. Yu, Y. *et al.* Controlled scalable synthesis of uniform, high-quality monolayer and few-layer MoS₂ films. *Scientific reports* **3**, 1866 (2013).
37. Lin, Z. *et al.* Controllable Growth of Large-Size Crystalline MoS₂ and Resist-Free Transfer Assisted with a Cu Thin Film. *Scientific reports* **5**, 18596 (2015).
38. V. Y., V. L. T., Boucaud, P., Debarre, D. & Bouchier, D. Kinetics of the heteroepitaxial growth of Ge on Si(001). *J. Vac. Sci. Technol. B* **20**, 1251–1258 (2002).
39. Baskaran, A. & Smereka, P. Mechanisms of Stranski-Krastanov growth. *J. Appl. Phys.* **111**, 044321 (2012).
40. Weiss, K. & Phillips, J. M. Calculated Specific Surface-Energy of Molybdenite (MoS₂). *Phys. Rev. B* **14**, 5392–5395 (1976).
41. Conway, B. E. & Tilak, B. V. Interfacial processes involving electrocatalytic evolution and oxidation of H₂, and the role of chemisorbed H. *Electrochim. Acta* **47**, 3571–3594 (2002).
42. Yu, Y. *et al.* Layer-dependent electrocatalysis of MoS₂ for hydrogen evolution. *Nano Lett.* **14**, 553–558 (2014).
43. Tao, L., Duan, X., Wang, C., Duan, X. & Wang, S. Plasma-engineered MoS₂ thin-film as an efficient electrocatalyst for hydrogen evolution reaction. *Chem Commun (Camb)* **51**, 7470–7473 (2015).
44. Seo, B. *et al.* Monolayer-Precision Synthesis of Molybdenum Sulfide Nanoparticles and Their Nanoscale Size Effects in the Hydrogen Evolution Reaction. *ACS nano* **9**, 3728–3739 (2015).
45. Xie, J. *et al.* Controllable disorder engineering in oxygen-incorporated MoS₂ ultrathin nanosheets for efficient hydrogen evolution. *J. Am. Chem. Soc.* **135**, 17881–17888 (2013).
46. Li, Y. B., Bando, Y. & Golberg, D. MoS₂ nanoflowers and their field-emission properties. *Appl. Phys. Lett.* **82**, 1962 (2003).
47. Late, D. J. *et al.* Pulsed laser-deposited MoS₂ thin films on W and Si: field emission and photoresponse studies. *ACS Appl. Mater. Interfaces* **6**, 15881–15888 (2014).
48. Forbes, R. G. Extraction of emission parameters for large-area field emitters, using a technically complete Fowler-Nordheim-type equation. *Nanotechnology* **23**, 095706 (2012).
49. Kim, S. *et al.* High-mobility and low-power thin-film transistors based on multilayer MoS₂ crystals. *Nat. Commun.* **3**, 1011 (2012).
50. Xiao, Z. *et al.* Field electron emission characteristics and physical mechanism of individual single-layer graphene. *ACS Nano* **4**, 6332–6336 (2010).

Acknowledgements

The authors would thank the support from Tsinghua Nanofabrication Technology Center. This research was supported by the National Basic Research Program (2011CBA00600), and the National Natural Science Foundation (61474072). This work was also funded by Tsinghua National Laboratory for Information Science and Technology (TNList).

Author Contributions

H.L. and S.Y. synthesized and characterized the materials. H.L. conducted the electrochemical characterization and field emission experiments. H.L. and H.W. conducted the TEM measurements and analysis. H.L. and H.W. wrote and edited the manuscript. The project was supervised by H.W. and H.Q.

Additional Information

Supplementary information accompanies this paper at <http://www.nature.com/srep>

Competing financial interests: The authors declare no competing financial interests.

How to cite this article: Li, H. *et al.* Synthesis and characterization of vertically standing MoS₂ nanosheets. *Sci. Rep.* **6**, 21171; doi: 10.1038/srep21171 (2016).



This work is licensed under a Creative Commons Attribution 4.0 International License. The images or other third party material in this article are included in the article's Creative Commons license, unless indicated otherwise in the credit line; if the material is not included under the Creative Commons license, users will need to obtain permission from the license holder to reproduce the material. To view a copy of this license, visit <http://creativecommons.org/licenses/by/4.0/>